

Tunable field depth: hyperbolic optical masks

LUIS LEDESMA-CARRILLO,¹ RAFAEL GUZMÁN-CABRERA,² CRISTINA M. GÓMEZ-SARABIA,³
MIGUEL TORRES-CISNEROS,¹ AND JORGE OJEDA-CASTAÑEDA^{1,*}

¹Electronics Department, Campus Irapuato-Salamanca, Universidad de Guanajuato, León, Mexico

²Electrical Department, Campus Irapuato-Salamanca, Universidad de Guanajuato, León, Mexico

³Digital Arts and Business Department, Campus Irapuato-Salamanca, Universidad de Guanajuato, León, Mexico

*Corresponding author: jojedacas@ugto.mx

Received 5 July 2016; revised 24 October 2016; accepted 27 October 2016; posted 28 October 2016 (Doc. ID 269866); published 29 November 2016

For controlling the depth of field, in an optical system working at full pupil apertures, we unveil the use of a pair of hyperbolic phase masks. For suitably framing our proposal, we link the Strehl ratio versus defocus with the area under the modulation transfer function (MTF). We show that by using hyperbolic phase masks, one can simultaneously reduce the impact of focus errors as well as increase the area under the MTF. We show that hyperbolic amplitude masks, with moderate absorption, can reduce the artifact noise caused by the use of phase masks. Finally, by exploiting the Lohmann–Alvarez technique, we describe the use of pairs of hyperbolic masks for governing field depth at fixed pupil apertures. © 2016 Optical Society of America

OCIS codes: (110.4850) Optical transfer functions; (110.4100) Modulation transfer function; (110.1758) Computational imaging; (110.2960) Image analysis; (070.0070) Fourier optics and signal processing.

<https://doi.org/10.1364/AO.56.00A104>

1. INTRODUCTION

For several imaging applications, it is desirable to govern field depth, while preserving a full pupil aperture, when gathering pictures of extended objects under noncoherent illumination. For these applications, it is convenient to recognize the existence of two different approaches for extending the depth of field in an optical system.

In the first approach, one aims to gather in single-snapshot 3D scenes while using optical masks that reduce the impact of focus error on the optical transfer function (OTF) of the optical system [1–4]. After recording the snapshot, one compensates any reduction in signal modulation by using a digital post processing algorithm [5,6].

In the second approach, one records several snapshots while purposely varying the focus error coefficient. After the recording stage, the snapshots are suitably combined for re-creating sharp images of the 3D scene [7,8]. It has been shown that this procedure can be represented by an equivalent OTF [9].

By using any of the two above approaches, one can surpass Hopkins' tolerance criterion to focus error [10]. However, for achieving this goal, it is convenient to recognize that the optical system must have a modulation transfer function (MTF) with the two following characteristics:

- In the absence of noise, the MTF should be different from zero within its passband.
- In the presence of noise, the values of the MTF should be equal to or greater than a given threshold value, for surpassing the variations of white noise.

For visualizing the above statements, in Fig. 1 we plot the MTF that is generated by three different pupil masks. For the three MTFs, the focus error coefficient is $W_{2,0} = 3\lambda$, where λ stands for the wavelength of the optical radiation [11,12].

The first curve, in blue, is the MTF of the clear pupil aperture. The second curve (in red) and the third curve (in violet) are the MTF for two different phase masks, to be specified in the paper. Also in Fig. 1, we draw four horizontal black lines. Each horizontal line represents the possible threshold values $L = 5\%$, 10% , 15% , and 20% . These percentage values describe the minimum modulation, which is needed for avoiding the presence of white noise.

From Fig. 1, we observe that each threshold line intercepts the MTFs, under discussion, at a different spatial frequency, denoted here as the effective cut-off frequency, Ω_e .

In Fig. 2, we plot the values of the effective cut-off spatial frequency as a function of the required threshold value, for the three MTFs in Fig. 1. From Fig. 2, we note that for the clear pupil aperture (the MTF in blue) the effective cut-off frequency is below 1/10 of the ideal cut-off frequency, 2Ω . Next, we observe that for the phase masks (MTFs in red and in violet) the effective cut-off frequency can easily surpass the values obtained when using a clear pupil.

From the results in Figs. 1 and 2, we claim that indeed some phase masks can increase field depth, even in the presence of white noise. Furthermore, also from Figs. 1 and 2, we recognize that one is tempted to select the phase mask that generates the

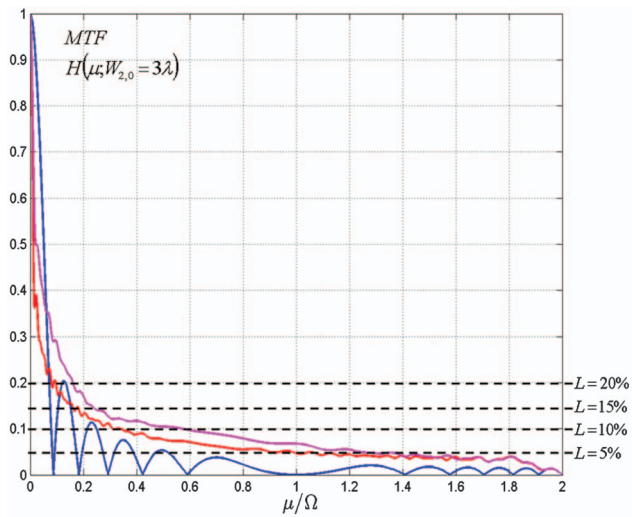


Fig. 1. MTF curves generated by three different optical masks, with the same focus error coefficient $W_{2,0} = 3\lambda$. The four horizontal lines, in black, depict the percentage threshold levels ($L = 5\%$, 10% , 15% , and 20%) for surpassing the presence of white noise.

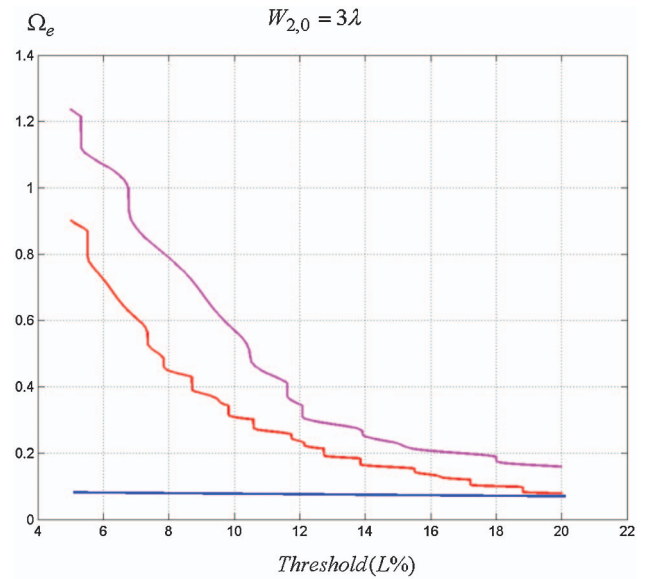


Fig. 2. Graphs depicting the variations of the effective cut-off frequency as a function of the threshold value for the MTFs in Fig. 1. For the three graphs, the value of the focus error coefficient is the same, $W_{2,0} = 3\lambda$.

violet curves, as a good choice for extending field depth. However, it is relevant to note the following.

Strictly speaking, the out-of-focus OTF is never equal to the in-focus OTF. Hence, there is not such a thing as focus invariance. Nonetheless, if one uses a suitable pupil mask, the square value of the difference between the out-of-focus OTF, $H(\mu; W_{2,0})$, and the in-focus OTF, $H(\mu; 0)$, can have rather small values. In mathematical terms, within the pass band $|\mu| \leq 2\Omega_e$, one can have that

$$|H(\mu; W_{2,0}) - H(\mu; 0)| \leq \epsilon; \quad \text{if } |W_{2,0}| \leq 3\lambda. \quad (1)$$

For the optical mask that generates the red curves in Figs. 1 and 2 the value is $\epsilon \leq 10^{-5}$, while for the optical mask that produces the violet curves (in Figs. 1 and 2) the value is only $\epsilon \leq 10^{-3}$.

Hence, the following questions arise. Is similarity between the defocused OTFs a good criterion for selecting masks that extend field depth? Or, as depicted in Fig. 2, should one select the masks for their capability to obtain higher values of the effective cut-off frequency? In this paper, we attempt to answer these questions.

Before that, it is pertinent to recognize that there is not a straightforward procedure for designing optical masks, which extend field depth. Nevertheless, one can outline some guiding principles that are useful for designing optical masks, which can generate MTFs that vary slowly with focus error [13,14].

As guiding principles, we note first that it is convenient to employ rectangular pupil apertures, for describing complex amplitude transmittances that are separable in Cartesian coordinates, as is depicted in Fig. 3.

We assume that the 2D complex amplitude transmittance of the pupil aperture can be expressed as the product of two equal separable functions. Each function acts along one axis. And the complex amplitude distribution along the horizontal axis is identical to the complex amplitude distribution along the

vertical axis. Therefore, for this type of pupil function, it is sufficient to discuss the 1D case.

The next guiding principle consists in recognizing that one can visualize all possible MTFs with variable focus error, by evaluating the RADAR ambiguity function of the pupil aperture [15].

Then, after evaluating and displaying the RADAR ambiguity, one can note the following. One can reduce the impact of focus error, if the pupil masks can generate ambiguity functions as those displayed in the last three pictures of Fig. 4. The main feature of these pictures is conveniently denoted as the bow-tie effect [16]. From Fig. 4, we observe that in the last three pictures the ambiguity function spreads, without zero values,

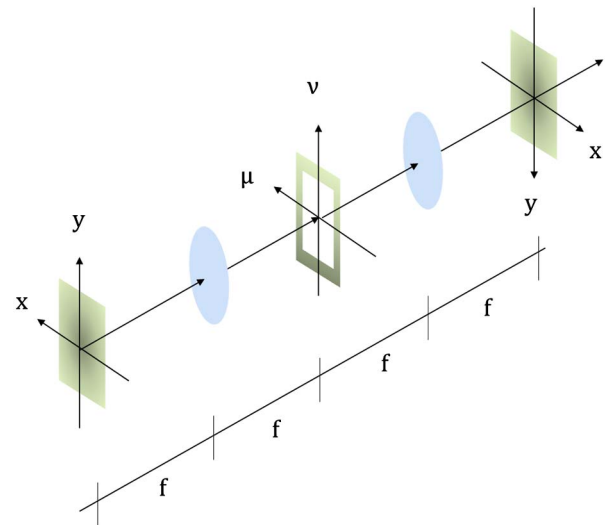


Fig. 3. Optical system that employs a rectangular pupil aperture. The complex amplitude transmittance of the pupil aperture is expressible as the products of two 1D complex amplitude transmittances.

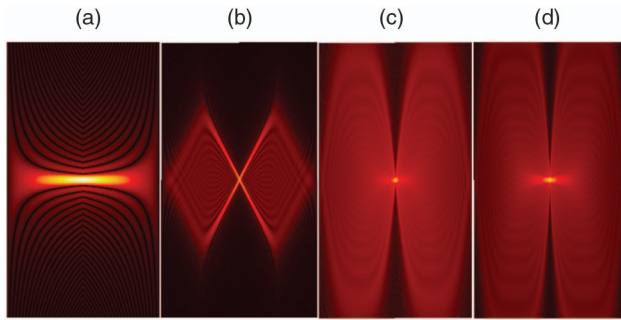


Fig. 4. Display of four different ambiguity functions associated to the following complex amplitude transmittances: (a) clear pupil aperture, (b) quadratic phase variation with odd symmetry, (c) fourth-order phase variation with odd symmetry, (d) sixth-order phase variation with odd symmetry.

along the vertical axis. This behavior is associated with the following mathematical result.

One can reduce by one-half the number of terms in the Taylor series expansion of the OTF versus focus error, provided that the pupil complex amplitude transmittance has Hermitian symmetry [17,18]. Hence, for transparent masks, the phase variations should be odd functions of the spatial frequency. And for attenuating masks, the amplitude variation should be even functions of the spatial frequency. By fulfilling this symmetry requirement, the MTF has a slow variation to focus error and consequently the ambiguity functions spread along the vertical axis.

Dowski and Cathey should be fully credited for introducing into optics a transparent mask with a cubic phase profile [19]. This phase function, with odd symmetry, was previously known in RADAR engineering [20]. Here we emphasize that there are many other possible phase functions, with odd symmetry, which can reduce the impact of focus error on the MTF [21].

Indeed, by recognizing explicitly the need of employing odd phase variations, one can identify fractional wavefronts, which can extend the field depth [22–25]. There are several other proposals for reducing the impact of focus error on the MTF [26–56]. For these applications, there are some useful digital restoration algorithms [57–59].

However, despite these relevant advances, there are few examples of pupil masks that can be mechanically tuned for governing field depth while preserving the same pupil aperture [60–65]. In this last set of publications, it has been recognized

that for implementing a tunable control of field depth, it is profitable to exploit the varifocal lens technique, due to Lohmann–Alvarez [66,67].

In a previous reference (see Ref. [60]), one of us coined the term phase conjugate pairs, for describing an optical device that uses a pair of phase masks that implement generalized versions of the Lohmann–Alvarez technique.

If one takes into account that the Lohmann–Alvarez technique can be phrased mathematically in terms of difference equations [68–70], one recognizes that the Lohmann–Alvarez technique is not restricted to monomial terms. Indeed, as is depicted in Table 2, sinusoidal phase variations and hyperbolic variations are also amiable for setting phase conjugate pairs.

In other words, in a reasonable induction process, one can consider that hyperbolic functions are suitable candidates for designing a pair of masks that can mechanically control field depth [71]. Out of curiosity, here we explore the possibility outlined in line 5 of Table 1.

In the first column of Table 1 we list four different functions with even symmetry. In column 2, we evaluate the finite difference that is obtained, after introducing a lateral displacement σ between a pair of the functions in column 1. Next, along column 3, by recognizing the results in column 2, we identify a phase function $\Psi(\mu)$ whose optical path difference is equal to the lower case letter “a”. Finally, we list the tunable phase delays that can be generated by lateral displacement of the masks forming a pair. From the last line and the last column of Table 1, it is clear that one can tune the maximum value of the optical path difference.

Based on the above descriptions, this paper has the three following aims:

Table 2. Decision Matrix Used for Selecting (Along the Columns) the Phase Profile of the Transparent Masks, and (Along the Rows) the Attenuation Profiles for the Amplitude Masks^a

Phase ⇒ Profile Amplitude			
Attenuations	Hyperbolic	Fractional	Cubic
↓			
Hyperbolic	Eq. (8)
Sub Gaussian	...	Eq. (9)	...
Gaussian	Eq. (10)

^aThe matrix elements specify the complex amplitude transmittance (phase and amplitude) of the masks discussed in this paper.

Table 1. Functions with Odd Symmetry Amiable for Setting Phase Conjugated Pairs, Allowing Optical Device Implementation That Can Govern the Depth of Field at Fixed Pupil Apertures

Suitable Function $F(\mu)$	Difference Equation $\Delta F(\mu; \sigma) = F(\mu + \frac{\sigma}{2}) - F(\mu - \frac{\sigma}{2})$	Mask's Phase Profile $\Psi(\mu)$	Tunable Phase Delays $\Delta\Psi(\mu)$
$F(\mu) = \mu^3$	$\Delta F(\mu; \sigma) = 3\sigma\mu^2 + \frac{\sigma^3}{4}$	$\Psi(\mu) = 2\pi a(\frac{\mu}{\Omega})^3$	$\Delta\Psi(\mu, \sigma) = 2\pi a\{(\frac{3\sigma}{\Omega})(\frac{\mu}{\Omega})^2 + 2(\frac{\sigma}{2\Omega})^3\}$
$F(\mu) = \mu^4$	$\Delta F(\mu; \sigma) = 4\sigma\mu^3 + \sigma^3\mu$	$\Psi(\mu) = 2\pi a(\frac{\mu}{\Omega})^4$	$\Delta\Psi(\mu, \sigma) = 2\pi a\{(\frac{4\sigma}{\Omega})(\frac{\mu}{\Omega})^3 + (\frac{\sigma}{\Omega})^3(\frac{\mu}{\Omega})\}$
$F(\mu) = \cos(\frac{\pi\mu}{2\Omega})$	$\Delta F(\mu; \sigma) = -2 \sin(\frac{\pi\sigma}{4\Omega}) \sin(\frac{\pi\mu}{2\Omega})$	$\Psi(\mu) = -\cos(\frac{\pi\mu}{2\Omega})$	$\Delta\Psi(\mu, \sigma) = 2 \sin(\frac{\pi\sigma}{4\Omega}) \sin(\frac{\pi\mu}{2\Omega})$
$F(\mu) = \cosh(\frac{\mu}{\Omega})$	$\Delta F(\mu; \sigma) = 2 \sinh(\frac{\sigma}{2\Omega}) \sinh(\frac{\mu}{\Omega})$	$\Psi(\mu) = \frac{\cosh(\frac{2\mu}{\Omega})}{\sinh(2\pi)}$	$\Delta\Psi(\mu, \sigma) = 2 \sinh(\frac{\sigma}{2\Omega}) \frac{\sinh(\frac{2\mu}{\Omega})}{\sinh(2\pi)}$

First, we reconnoiter the use of a transparent mask whose phase profile follows a hyperbolic sinusoidal profile, for reducing the influence of focus errors on the MTF.

Second, we explore use of a moderate attenuating hyperbolic mask, for reducing the artifact noise introduced in the MTF, by the use of phase masks.

Third, we connect our explorations for describing the use of hyperbolic pairs, for controlling the optical path difference on the phase mask. We show also that the same procedure applies for tuning the damping factor of attenuating masks with hyperbolic profiles.

For properly framing our present explorations, in Section 2, we link explicitly the Strehl ratio versus focus error with MTF image quality criteria. This analytical link allows us to consider, as a figure of merit, the area under the OTF. In Section 3, we discuss the optical characteristics of phase masks with asymmetrical hyperbolic profiles. In Section 4, we describe the characteristics of a moderate absorbing mask, which uses filters with symmetrical hyperbolic profile for reducing artifact noise. In Section 5, we discuss a method for mechanically controlling field depth by laterally displacing a pair of hyperbolic masks. And finally in Section 6, we express our conclusions.

2. RELATING IMAGE QUALITY CRITERIA

For the sake of completeness of our discussion on masks that extend field depth, in what follows we link explicitly the Strehl ratio versus focus error with MTF image quality criteria.

As stated in the introduction, we only require to analyze the 1D version of the generalized pupil function, denoted here $P(\mu; W_{2,0})$. As before, $W_{2,0}$ stands for the focus error coefficient. Then, the irradiance distribution of the point spread function (PSF) is obtained in two steps,

$$p(x; W_{2,0}) = \int_{-\Omega}^{\Omega} P(\mu; W_{2,0}) \exp(i2\pi\mu x) d\mu, \tag{2}$$

$$h(x; W_{2,0}) = |p(x; W_{2,0})|^2.$$

As before, in Eq. (2) μ stands for the spatial frequency coordinate along the 1D pupil aperture. Next, we recognize that Eq. (2) can also be written as

$$h(x; W_{2,0}) = \int_{-\Omega}^{\Omega} H(\mu; W_{2,0}) \exp(i2\pi\mu x) d\mu. \tag{3a}$$

In Eq. (3a) we denote $H(\mu; W_{2,0})$ as the OTF of the optical system. By using the well-known Duffieux formula, Eq. (3a) can also be expressed as

$$H(\mu; W_{2,0}) = \int_{-\frac{\Omega}{2}(1-\frac{\mu}{2\Omega})}^{\frac{\Omega}{2}(1-\frac{\mu}{2\Omega})} P\left(\nu + \frac{\mu}{2}; W_{2,0}\right) \times P^*\left(\nu - \frac{\mu}{2}; W_{2,0}\right) \exp(i2\pi\mu x) d\nu. \tag{3b}$$

For classical optical systems, it is well known that the maximum value of the irradiance PSF is on-axis. However, due to the symmetry condition discussed in the introduction, this consideration does not apply for the masks that increase field depth. Now, with this warning in mind, we write down the on-axis value of the PSF.

$$h(0; W_{2,0}) = \int_{-\Omega}^{\Omega} H(\mu; W_{2,0}) d\mu = 2 \int_0^{\Omega} \text{Re}\{H(\mu; W_{2,0})\} d\mu. \tag{4a}$$

In Eq. (4a) we use the shorthand notation $\text{Re}\{\cdot\}$ for taking the real part of the OTF. The real part is an even function. Trivially, in the absence of focus errors, the on-axis PSF is

$$h(0, 0) = 2 \int_0^{\Omega} \text{Re}\{H(\mu; 0)\} d\mu. \tag{4b}$$

From Eq. (4) we obtain the following expression for the Strehl ratio for focus errors:

$$s(W_{2,0}) = \frac{\int_0^{\Omega} \text{Re}\{H(\mu; W_{2,0})\} d\mu}{\int_0^{\Omega} \text{Re}\{H(\mu; 0)\} d\mu}. \tag{5}$$

Surely the expression in Eq. (5) has been reported elsewhere. However, we were unable to trace proper references. Next, it is important to recognize that since the imaginary part of the OTF is an odd function, then

$$\int_{-\Omega}^{\Omega} \text{Im}\{H(\mu; W_{2,0})\} d\mu = 0. \tag{6a}$$

However, we notice that

$$t(W_{2,0}) = \frac{\int_0^{\Omega} \text{Im}\{H(\mu; W_{2,0})\} d\mu}{\int_0^{\Omega} \text{Im}\{H(\mu; 0)\} d\mu} \neq 0. \tag{6b}$$

Now, it is apparent from Eqs. (5) and (6) that both the Strehl ratio and the just above defined t ratio must be taken into account when evaluating the performance of masks.

Here we consider the above two ratios by using the area under the MTF versus focus error, as a figure of merit, namely

$$A(W_{2,0}) = \int_0^{\Omega} |H(\mu; W_{2,0})| d\mu. \tag{7}$$

In what follows, we apply Eq. (7) for making useful comparisons between optical masks that reduce the impact of focus error. However, in our discussions, we do not apply alone either the Strehl ratio in Eq. (5) or the t ratio in Eq. (6b).

3. MASKS FOR REDUCING THE INFLUENCE OF THE FOCUS ERRORS

For discussing our proposal, it is convenient to write the generalized pupil function as follows:

$$P(\mu; W_{2,0}; a; c) = \exp\left\{i2\pi a \left[\frac{\sinh\left(2\pi\frac{\mu}{\Omega}\right)}{\sinh(2\pi)}\right]\right\} \exp\left\{-c \left[\frac{\cosh\left(2\pi\frac{\mu}{\Omega}\right)}{\cosh(2\pi)}\right]\right\} \times \exp\left\{i2\pi\frac{W_{2,0}}{\lambda} \left(\frac{\mu}{\Omega}\right)^2\right\} \text{rect}\left(\frac{\mu}{2\Omega}\right). \tag{8}$$

In Eq. (8), the first factor describes the hyperbolic phase variations under consideration. As pointed out in the introduction, the phase variation should be described by odd functions, which are amiable for implementing the Lohmann–Alvarez technique. We believe that this is the first time that a hyperbolic phase variation is proposed for extending field depth.

The second term considers possible amplitude attenuations. Again, as was indicated in the introduction, the amplitude variations are described by even functions. To the best of our knowledge, this is the second time that a hyperbolic attenuation is proposed for extending field depth (see Ref. [71]).

The third term in Eq. (8) denotes the presence of focus errors. The finite size of the pupil aperture is expressed as a rectangular window. μ denotes the spatial frequency in the pupil aperture. Its maximum value is the cut-off spatial frequency Ω .

We note that the complex amplitude transmittance in Eq. (8), a denotes the maximum value for the optical path difference (in units of the wavelength λ) of the phase profile. We use c for denoting the damping coefficient in the amplitude attenuations. These two parameters are unknown at this stage. However, we have performed several numerical simulations for finding some recommended values.

For placing our proposal in a proper context, along the columns of Table 2, we describe our three possible choices for selecting the phase profiles. In a similar manner, along the lines of Table 2, we describe our three possible choices for selecting the amplitude attenuations.

For example, the matrix element, at the first column and the first row, is the complex amplitude transmittance in Eq. (8).

The matrix element, at the second column and the second row, is the complex amplitude transmittance in Eq. (9). Finally, the matrix element, at the third column and the third row, is the complex amplitude distribution in Eq. (10).

$$P(\mu; W_{2,0}; a; c) = \exp \left\{ i2\pi a \left[\operatorname{sgn}(\mu) \left(\frac{\mu}{\Omega} \right)^{3.36} \right] \right\} \exp \left\{ -c \left[\frac{\mu}{\Omega} \right]^{1.532} \right\} \times \exp \left\{ i2\pi \frac{W_{2,0}}{\lambda} \left(\frac{\mu}{\Omega} \right)^2 \right\} \operatorname{rect} \left(\frac{\mu}{2\Omega} \right). \quad (9)$$

In Eq. (9), the first factor describes an odd phase variation of the fractional order 3.36, while the second factor expresses the amplitude transmittance of a sub Gaussian mask, with an order

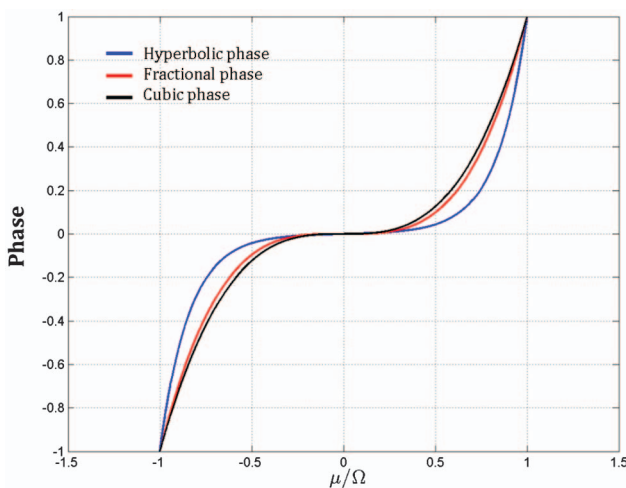


Fig. 5. Phase profiles associated to the optical masks described by the first factor in Eqs. (8)–(10), respectively. The blue curve is a hyperbolic sine variation; the red curve is a phase profile of fractional order and slightly different from the cubic phase variation in black.

of 1.532 (see, for example, Ref. [71]). The following generalized pupil function is

$$P(\mu; W_{2,0}; a; c) = \exp \left\{ i2\pi a \left(\frac{\mu}{\Omega} \right)^3 \right\} \exp \left\{ -c \left(\frac{\mu}{\Omega} \right)^2 \right\} \times \exp \left\{ i2\pi \frac{W_{2,0}}{\lambda} \left(\frac{\mu}{\Omega} \right)^2 \right\} \operatorname{rect} \left(\frac{\mu}{2\Omega} \right). \quad (10)$$

In Eq. (10), the first factor describes the cubic phase mask, and the second factor expresses the amplitude transmittance of a Gaussian mask. To the best of our knowledge, this amplitude masks was first proposed in Ref. [56]. In Fig. 5, we plot the phase profiles in Eqs. (8)–(10), while in Fig. 6, we plot the amplitude variations in Eqs. (8)–(10).

As is depicted in Fig. 7, we have evaluated numerically the MTFs of the generalized pupil function in Eq. (8), for several values of the coefficient a , while keeping constant $c = 0$, as well as the value of the focus error coefficient, $W_{2,0} = 3\lambda$. After performing several numerical evaluations, we select the value $a = 17$.

Here we recognize that some care should be taken when considering the maximum value of the optical path difference, which is equal to $a = (N - 1)e_0/\lambda$, where N stands for the value of the refractive index of the material used for building the refractive element, e_0 denotes the maximum thickness of the optical mask, and λ represents the wavelength of the optical radiation. This means that if $N = 1.5$ (for a given value of λ) and $a = 17$, then the maximum thickness of the optical mask is 34λ . This is a reasonable value for a refractive element. However, we do not claim that this value ($a = 17$) is an optimum value.

In a similar manner, as depicted in Fig. 8, we have evaluated numerically the MTFs of the generalized pupil function in Eq. (8), for several values of the dimensionless coefficient c , while keeping constant $a = 0$, as well as the value of the focus error coefficient, $W_{2,0} = 3\lambda$.

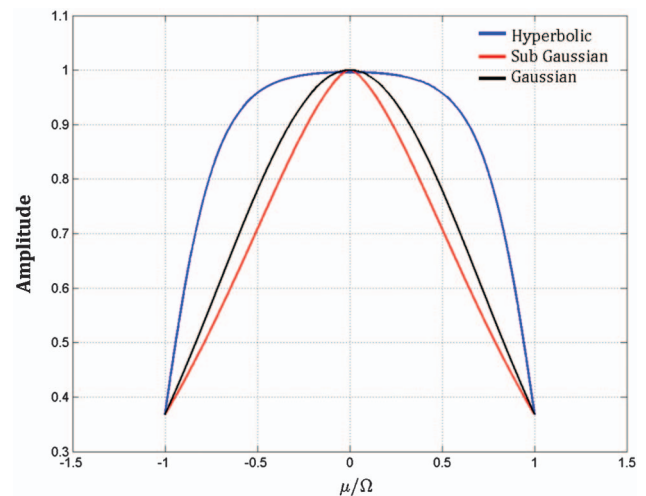


Fig. 6. Amplitude transmittances associated to the optical masks in Eqs. (8)–(10). The blue curve is a hyperbolic cosine variation, the red curve describes a sub Gaussian variation, and the black curve describes a Gaussian attenuation.

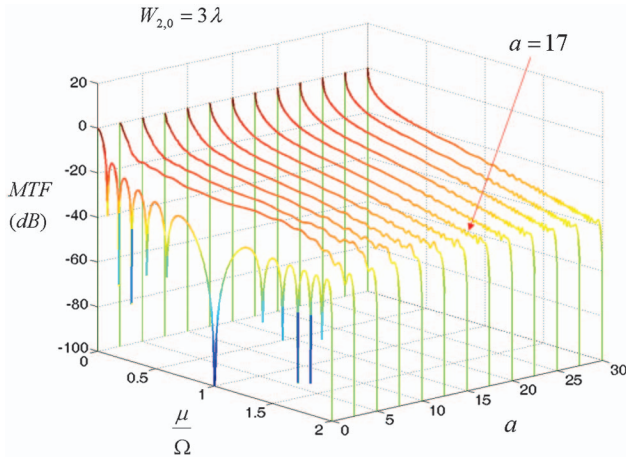


Fig. 7. Variations of the MTFs (in dB) as a function of the normalized spatial frequency, μ/Ω , and the parameter a representing the optical path difference in units of λ . We note that the MTF changes slowly if $a \geq 15$. Based on this picture we have selected the value $a = 17$. [Admittedly, we cannot claim that this value is an optimum value.]

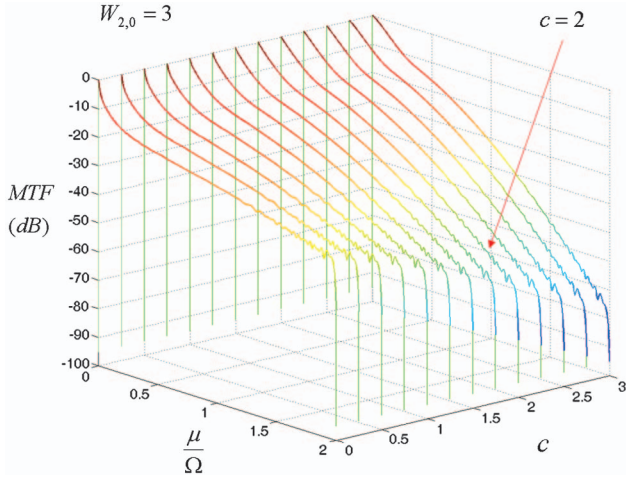


Fig. 8. Variations of the MTFs (in dB) as a function of both the normalized spatial frequency, μ/Ω , and the parameter c representing the attenuation factor of the amplitude mask. MTF changes slowly if $c \geq 1.5$. We have selected the value $c = 2$. [However, again, we do not claim that this value is an optimum value.]

After these numerical evaluations we select the value $c = 2$, which represents a moderate attenuation factor. *Again, we do not claim that the value $c = 2$ is an optimum value.*

After the selection of the parameters a and c for evaluating the performance of the proposed masks, we perform the following comparisons. For testing the slow variations of the MTF versus focus error, we evaluate the MTFs that are obtained if the generalized pupil function is described by Eq. (8), for $a = 17$ and $c = 0$. Our results are displayed in Fig. 9. From Eq. (1) and from the curves in Fig. 9, we have that for the hyperbolic sine mask

$$|H(\mu; W_{2,0}) - H(\mu; 0)| \leq 10^{-1}; \quad \text{if } |W_{2,0}| \leq 3\lambda. \quad (11)$$

For a phase mask of fractional order, as that in Eq. (9) with $a = 17$ and $c = 0$, one obtains that

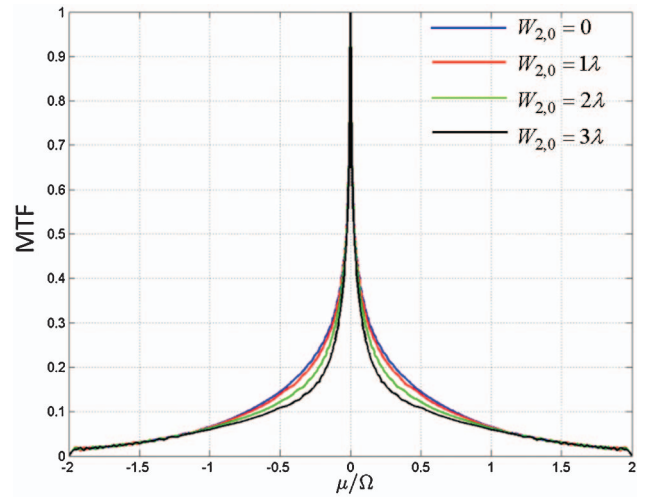


Fig. 9. Graphical comparisons of the numerically evaluated MTFs, for the hyperbolic phase mask in Eq. (8), when setting $a = 17$ and $c = 0$.

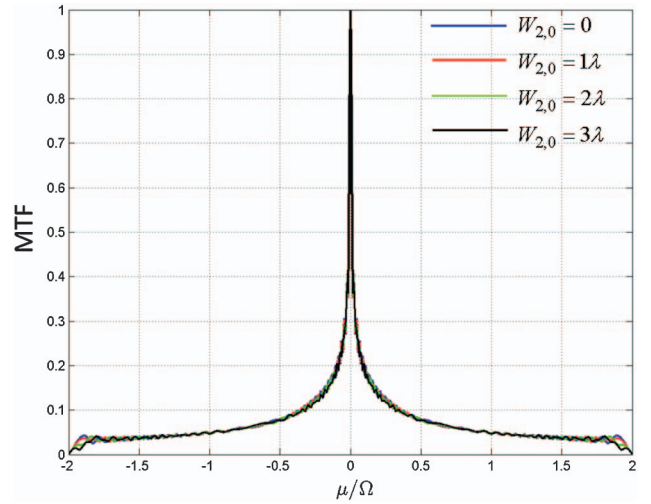


Fig. 10. Graphical comparisons of the numerically evaluated MTFs, for the fractional phase mask in Eq. (9), when setting $a = 17$ and $c = 0$. Along the trend curves of the MTFs, one can notice unwanted oscillations, denoted here as artifact noise.

$$|H(\mu; W_{2,0}) - H(\mu; 0)| \leq 10^{-3}; \quad \text{if } |W_{2,0}| \leq 3\lambda. \quad (12)$$

By making comparisons between Eqs. (11) and (12), as well as between Figs. 9 and 10, one is tempted to conclude that the phase mask of fractional order over performs the hyperbolic phase mask. However, by looking at the results in Fig. 11, from the viewpoint of the threshold levels, we decide to evaluate the effective cut-off frequency of these masks, as is reported in Fig. 12.

It is clear from Fig. 12 that for a low threshold ($L \leq 5\%$) the effective cut-off spatial frequency has lower values for the hyperbolic phase mask than for the other phase masks. However, for middle and high threshold values, the reverse is true. Hence,

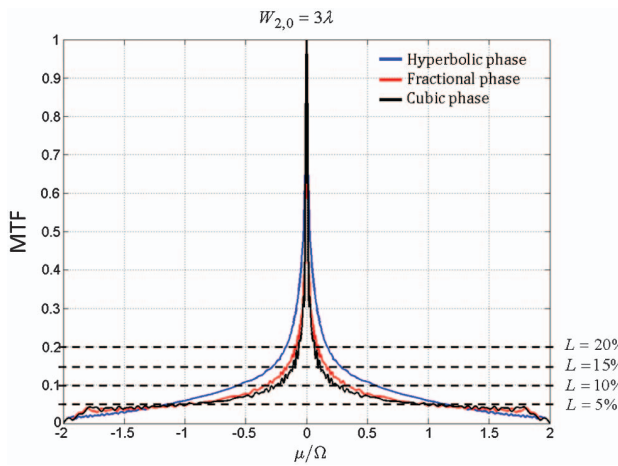


Fig. 11. Graphical comparisons between the MTFs of the hyperbolic phase mask (in blue), a phase mask of fractional order (in red), and the cubic phase mask (in black), when setting $a = 17$, $c = 0$, and $W_{2,0} = 3\lambda$.

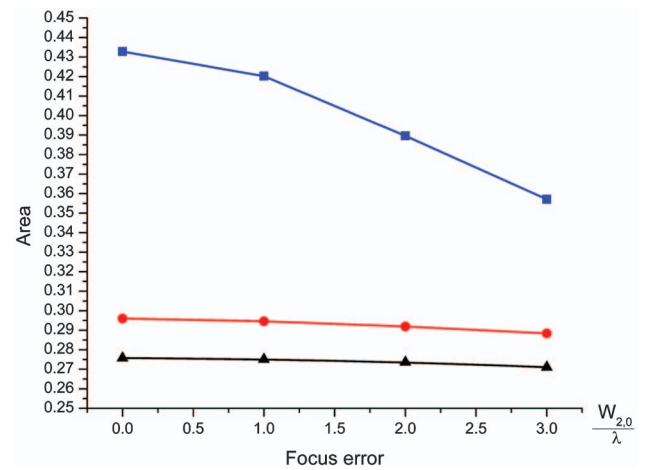


Fig. 13. Areas under the MTF versus focus errors for the hyperbolic phase mask (in blue), a phase mask of fractional order (in red), and the cubic phase mask (in black), if $a = 17$, $c = 0$ and $0 \leq W_{2,0} \leq 3\lambda$.

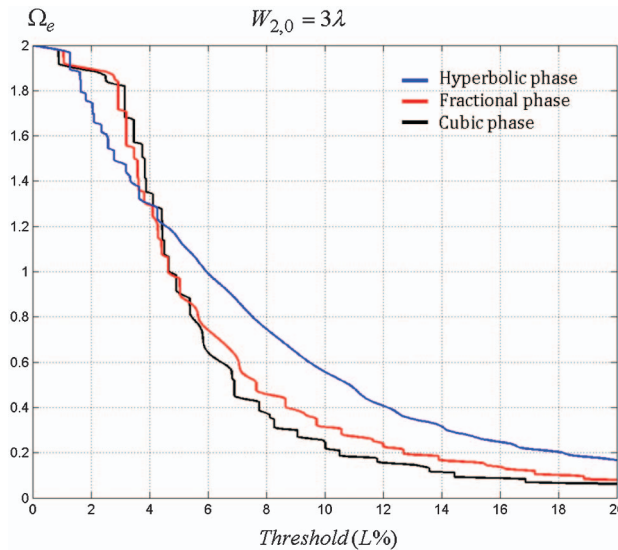


Fig. 12. Effective cut-off spatial frequency versus threshold values for the hyperbolic phase mask (in blue), a phase mask of fractional order (in red), and the cubic phase mask (in black), when setting $a = 17$, $c = 0$, and $W_{2,0} = 3\lambda$.

we claim that the hyperbolic phase mask has a better signal-to-noise ratio performance than the other phase masks.

Furthermore, as depicted in Fig. 13, if one keeps constant the value of the parameters $a = 17$ and $c = 0$, the area under the MTF is higher for the hyperbolic mask than for other phase masks.

It is clear from Fig. 13 that if a MTF varies slowly with focus error, its area under the MTF remains practically constant, as expected. However, this feature does not guarantee that the area under the MTF has a high value, as in the blue curve.

To visualize these latter results differently, in Fig. 14, we group the images that can be obtained, if one employs the masks under discussion.



Fig. 14. Numerically evaluated out-of-focus images, which are obtained if the cut-off spatial frequency is $\Omega_e = (1.5) \Omega$, and when using (a) the clear pupil aperture, (b) the hyperbolic optical mask, and (c) the cubic phase mask.

Along the columns of Fig. 14, the focus error coefficient increases in steps of one wavelength, starting from $W_{2,0} = 0$. Along the first line of Fig. 14, we display the images that can be obtained when introducing focus error, if the optical system has a clear pupil aperture. Along the second line of Fig. 14, we show the numerical simulations, if the optical system has the hyperbolic mask in Eq. (8), for $a = 17$ and $c = 0$. And along the third line of Fig. 14, we show the images that can be obtained, if the optical system has a cubic phase mask, as in Eq. (3) for $a = 17$ and $c = 0$. For generating these pictures, we consider that the threshold level is $L = 4\%$, and, consequently, we consider that the cut-off spatial frequency is $\Omega_e = (1.5) \Omega$.

The visual displays, in Fig. 14, show that in these conditions, the hyperbolic mask generates images with higher visual fidelity than those generated by either the phase mask of fractional order or the cubic phase mask. However, there appears to

be some experimental evidence that the area under the MTF is not a good figure of merit in ophthalmology [72].

In the following section, we show that the results in Figs. 11, 12, and 14 can be improved, if one uses (with the phase mask) a second mask with moderate attenuations.

4. REDUCING THE PRESENCE OF ARTIFACT NOISE

Several authors have noted that whenever one uses a phase filter for decreasing the impact of focus error on the MTF, one generates unwanted oscillations around the trend curve describing the MTF, as can be observed in Figs. 9–11.

For reducing the presence of this type of artifact noise, the use of a Gaussian apodizer with moderate attenuation (which can be tunable) together with the phase masks has been suggested. See, for example, Ref. [56]. Of course, other types of amplitude masks can be used for reducing this type of artifact noise. See, for example, Ref. [64]. In what follows, for reducing the presence of artifact noise we explore the use of three different attenuating masks, when used with the hyperbolic phase masks. Admittedly, we are narrowing our discussion, since we are focusing on the optical behavior of the hyperbolic phase masks. However, in Ref. [23], there are detailed discussions on the use of phase masks with fractional order (including the cubic phase mask) in combination with sub Gaussian masks and with super Gaussian masks.

We can trace our next exploration in the decision matrix in Table 2, as moving down along the matrix lines, while staying at the first column. Along the decision matrix we do not move along the columns, since this is beyond our present scope.

By making a comparison between Figs. 11 and 15, we observe that the amplitude masks do reduce the presence of artifact noise. It is not straightforward to notice if there is an increment in the area under the MTF curves. Hence, we evaluate the area under the MTF, of the above combinations, for

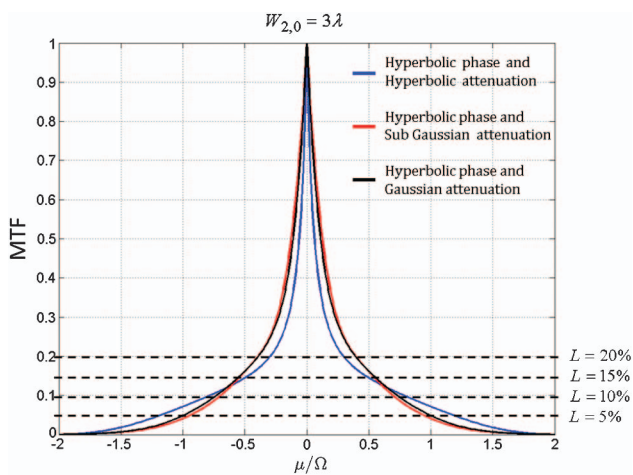


Fig. 15. Graphical comparisons between the MTFs of the hyperbolic phase mask, when it is used with the three following attenuation masks: in blue, the hyperbolic cosine mask in Eq. (8); in red, the sub Gaussian mask in Eq. (9); and in black, the Gaussian mask in Eq. (10). These results are obtained if the optical path difference is $a = 17$, the damping factor is $c = 2$, and the focus error coefficient is $W_{2,0} = 3\lambda$.

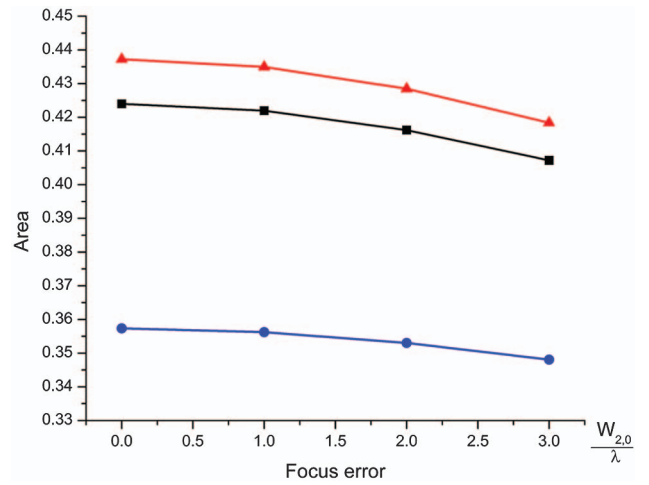


Fig. 16. Area under the MTF versus focus error. As in Fig. 15, we are denoting in blue the combination hyperbolic phase and hyperbolic attenuation; in red the hyperbolic phase and sub Gaussian attenuation; and in black the hyperbolic phase and Gaussian attenuation. These results are obtained for $a = 17$, and $c = 2$.

several values of the focus error coefficient. Our numerical evaluations are shown in Fig. 16.

Here again, it is clear from Fig. 16 that if a MTF varies slowly with focus error, its area under the MTF remains practically constant, as expected. However, this feature does not guarantee that the area under the MTF has a high value, as in the red curve.

Furthermore, from Fig. 16, we recognize that the combination hyperbolic phase and sub Gaussian attenuation yields to the highest rate of change $\Delta \text{Area} / \Delta W_{2,0} = -0.062$.

However, the same combination produces the highest values of the area under the MTF, namely $41.8 \leq A(W_{2,0}) \leq 43.75\%$. These results are valid, provided that $|W_{2,0}| \leq 3\lambda$. Within this range of values, we claim that the area under the MTF is a good figure of merit. From the above results, one expects that the combination hyperbolic phase and sub Gaussian attenuation can generate images of higher visual fidelity than the images in Fig. 14. For validating this guess, we evaluate the images depicted in Fig. 17.

From Figs. 16 and 17, we claim that the combination of hyperbolic phase and sub Gaussian attenuation can generate a high area under the MTF, and that this combination increases visual image fidelity.

5. TUNABLE DEVICES: HYPERBOLIC PAIRS

When designing optical masks that extend field depth, there are three main challenges, which can be described heuristically as follows. First, if one wishes to preserve light-gathering power, one avoids the trivial solution of closing the pupil aperture. In other words, one uses phase-only masks, typically, in the form of non-heavy, refractive elements with reasonable thickness.

Second, if one wishes to avoid artifact noise on the MTF, one must use an attenuation mask, which will reduce light-gathering power by a reasonable amount.

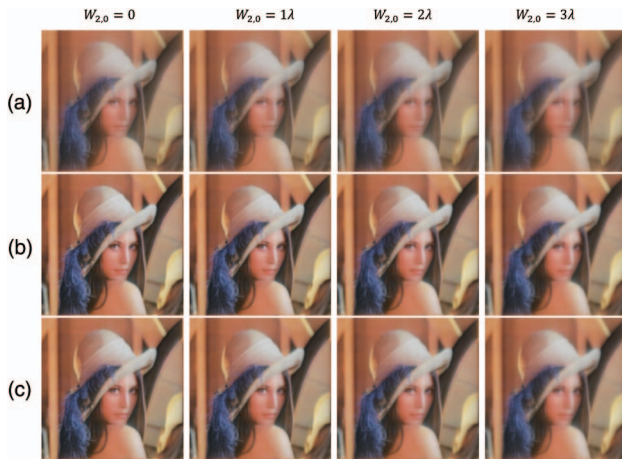


Fig. 17. Numerically evaluated out-of-focus images, which are obtained when using the hyperbolic phase mask with (a) a hyperbolic apodizer, (b) a sub Gaussian apodizer, and (c) a Gaussian apodizer. In the three cases $a = 17$ and $c = 2$. Along the columns the focus error coefficient increases in steps of one wavelength.

Third, one needs a technique for adjusting field depth, without modifying the two previous requirements.

In this section we aim to set tunable devices by employing two static masks, which form a pair. The main advantages of this type of device are that by forming a pair of phase masks the optical system can work at full pupil aperture, and, consequently, one can preserve light-gathering power. Yet, it is possible to govern field depth.

Furthermore, by using a pair of amplitude masks the optical system preserves resolution; yet, one can reduce the presence of artifact noise. However, in this case one reduces light-gathering power.

Finally, we notice that one can adjust field depth (at full pupil apertures) by mechanically shifting the elements forming the pair.

To our end, in what follows, we discuss an extension of the optical technique proposed, independently and simultaneously, by Lohmann and Alvarez (see Refs. [66,67,73,74]).

Here, for controlling the maximum value of the optical path difference, we suggest using the following pair of complex amplitude transmittances:

$$\begin{aligned} Q_1(\mu; b) &= \exp \left\{ i2\pi b \left[\cosh \left(2\pi \frac{\mu}{\Omega} \right) \right] \right\} \text{rect} \left(\frac{\mu}{4\Omega} \right), \\ Q_2(\mu; b) &= \exp \left\{ -i2\pi b \left[\cosh \left(2\pi \frac{\mu}{\Omega} \right) \right] \right\} \text{rect} \left(\frac{\mu}{4\Omega} \right). \end{aligned} \quad (13)$$

In Eq. (13) b denotes the maximum value of the optical path difference, at each element of the pair. In what follows, we related this parameter with the parameter a in Eq. (8) by recognizing the following two physical restrictions:

- (1) If the refractive index is $N = 1.5$ for a given value of λ and $a = 17$, the maximum thickness of the optical mask is 34λ .
- (2) The elements of the pair must be larger than the pupil aperture.

If one places together the two elements of the pair as in Eq. (13), and if one introduces an in-plane displacement

between them (say, by the spatial frequency σ). Then, the overall complex amplitude transmittance is

$$\begin{aligned} Q_{\text{phase}}(\mu; \sigma; b) &= Q_1 \left(\mu + \frac{\sigma}{2}; b \right) Q_2 \left(\mu - \frac{\sigma}{2}; b \right) \text{rect} \left(\frac{\mu}{2\Omega} \right) \\ &= \exp \left\{ i2\pi b \left[\cosh \left(2\pi \frac{\mu + \frac{\sigma}{2}}{\Omega} \right) - \cosh \left(2\pi \frac{\mu - \frac{\sigma}{2}}{\Omega} \right) \right] \right\} \text{rect} \left(\frac{\mu}{2\Omega} \right) \\ &\times \exp \left\{ i2\pi \left[2b \sinh \left(\pi \frac{\sigma}{\Omega} \right) \right] \sinh \left(2\pi \frac{\mu}{\Omega} \right) \right\} \text{rect} \left(\frac{\mu}{2\Omega} \right). \end{aligned} \quad (14)$$

The result in Eq. (14) is in agreement with the difference equations discussed in Table 1. If one compares Eq. (8) and Eq. (14) it is apparent that one can control the maximum value of the optical path difference as follows:

$$a = 2b \sinh(2\pi) \sinh \left(\pi \frac{\sigma}{\Omega} \right). \quad (15)$$

Then, from Eq. (15) we find that for achieving the value $a = 17$, with a lateral displacement of $\sigma = \Omega/10$, it is necessary that each element of the pair has an optical path difference of $b = 0.0994$.

Now, we proceed to evaluate the maximum thickness e_1 of the elements forming the pair, by recognizing that $b = (N - 1)e_1/\lambda$. Again, if $N = 1.5$ for a given value of λ and $a = 17$, the maximum thickness of the optical mask is around $\lambda/2$. This is a reasonable value for fabricating a non-heavy optical element.

Next, we recognize that a similar procedure can be exploited for controlling the damping coefficient in the amplitude masks. For this application, we propose using the following amplitude transmittances:

$$\begin{aligned} Q_3(\mu; b) &= \exp \left\{ -g \sinh \left(2\pi \frac{\mu}{\Omega} \right) \right\} \text{rect} \left(\frac{\mu}{4\Omega} \right), \\ Q_4(\mu; b) &= \exp \left\{ -g \left[1 - \sinh \left(2\pi \frac{\mu}{\Omega} \right) \right] \right\} \text{rect} \left(\frac{\mu}{4\Omega} \right). \end{aligned} \quad (16)$$

In Eq. (16) g denotes the maximum value of the damping coefficient at each element of the pair. In what follows, we related the parameter g with the parameter c in Eq. (8).

However, before that, we note that by placing together the two elements of the pair, in Eq. (14), and by introducing an in-plane displacement between them (say, by the spatial frequency σ) then the overall complex amplitude transmittance is

$$\begin{aligned} Q_{\text{amp}}(\mu; \sigma; b) &= Q_3 \left(\mu + \frac{\sigma}{2}; b \right) Q_4 \left(\mu - \frac{\sigma}{2}; b \right) \text{rect} \left(\frac{\mu}{2\Omega} \right) \\ &= \exp \left\{ -g \left[\sinh \left(2\pi \frac{\mu + \frac{\sigma}{2}}{\Omega} \right) - \sinh \left(2\pi \frac{\mu - \frac{\sigma}{2}}{\Omega} \right) \right] \right\} \text{rect} \left(\frac{\mu}{2\Omega} \right) \\ &\times \exp \left\{ - \left[2g \sinh \left(\pi \frac{\sigma}{\Omega} \right) \right] \cosh \left(2\pi \frac{\mu}{\Omega} \right) \right\} \text{rect} \left(\frac{\mu}{2\Omega} \right). \end{aligned} \quad (17)$$

If one compares Eqs. (8) and (17) and neglects the constant attenuation factors, it is apparent that the maximum value of the damping coefficient is

$$c = 2g \cosh(2\pi) \sinh \left(\pi \frac{\sigma}{\Omega} \right). \quad (18)$$

Therefore, by using Eq. (18), we find that for achieving an overall damping factor of $c = 2$, each element of the pair must

have a damping factor $g = 0.0117$, indeed a low value for an attenuation mask, as we discuss next. For assessing the loss in light-gathering power, one needs to evaluate the integral

$$T = \frac{1}{2\Omega} \int_{-\Omega}^{\Omega} |P(\mu; a; c; W_{2,0})|^2 d\mu. \quad (19)$$

By substituting Eq. (8) in Eq. (19) one obtains that, for the hyperbolic masks, the light-gathering power is

$$T = \frac{1}{2\Omega} \int_{-\Omega}^{\Omega} \exp \left\{ -2c \left[\frac{\cosh(2\pi \frac{\mu}{\Omega})}{\cosh(2\pi)} \right] \right\} d\mu. \quad (20)$$

Trivially, if $c = 0$ the light throughput is equal to unity. If the damping factor is $c = 2$, the light throughput is decreased from unity to 0.6869. Hence, from the viewpoint of light throughput, for a square aperture this is equivalent to halving the area of the pupil aperture. Yet, from the viewpoint of resolution one preserves the full pupil aperture. This is the cost to be paid for reducing the influence of artifact noise.

6. CONCLUSIONS

For controlling the field depth, we have presented a new family set of spatial filters, denoted here as hyperbolic masks. We have shown that even in the presence of white noise, these masks can reduce the influence of focus error.

For properly framing our proposal, we have argued that this type of mask can be identified by taking into account that the Lohmann–Alvarez technique can be described mathematically by finite difference calculus. Next, we have recognized that hyperbolic functions are suitable candidates for this treatment.

We have shown that one can reduce the influence of focus errors by using transparent masks, which incorporate phase delays with a hyperbolic sine profile. Furthermore, we claim that indeed these phase masks can increase field depth, even in the presence of white noise.

For evaluating the performance of this type of mask, we have linked the image quality criterion for the PSF with some MTF criteria. This link was used as a motivation for proposing the area under the MTF versus focus error as a figure of merit.

We have shown that the proposed hyperbolic phase masks can have a high area under the MTF, and at the same time the hyperbolic masks reduce the influence of focus error on the MTF.

Our numerical simulations indicate that, due to the high area under the MTF curves, the hyperbolic masks can gather images with higher visual fidelity than previously reported masks for extending field depth.

Next, we have noted that when increasing field depth by using phase masks, one introduces artifact noise on the MTF. We have noted that this type of noise can be reduced by using amplitude masks with moderate absorption. We have shown that the use of hyperbolic amplitude masks can reduce this type of artifact noise.

Specifically, we have reported that by using a hyperbolic phase mask, together with a sub Gaussian apodizer, one obtains a high area under the MTF, together with a moderate variation of the MTF with focus error, and a reduction of artifact noise.

We have shown that by using the Lohmann–Alvarez method, one can mechanically govern field depth, at full pupil apertures, if one uses suitable pairs of hyperbolic masks.

For the hyperbolic phase masks, the elements of the transparent pair can have a thickness of around $\lambda/2$. The elements of the amplitude pair can reduce light throughput by one-half. However, both pairs preserve the size of the full aperture.

Along with our contribution, we have reported several numerical comparisons for illustrating the main advantages and disadvantages of hyperbolic masks.

REFERENCES

1. M. Mino and Y. Okano, "Improvement in the OTF of a defocused optical system through the use of shaded apertures," *Appl. Opt.* **10**, 2219–2225 (1971).
2. J. Ojeda-Castañeda, L. R. Berriel-Valdos, and E. L. Montes, "Line spread function relatively insensitive to defocus," *Opt. Lett.* **8**, 458–460 (1983).
3. G. Indebetow and H. Bai, "Imaging with Fresnel zone pupil masks: extended depth of field," *Appl. Opt.* **23**, 4299–4302 (1984).
4. J. Ojeda-Castañeda, R. Ramos, and A. Noyola-Isgleas, "High focal depth by apodization and digital restoration," *Appl. Opt.* **27**, 2583–2586 (1988).
5. W. T. Cathey and E. R. Dowski, "New paradigm for imaging systems," *Appl. Opt.* **41**, 6080–6092 (2002).
6. R. Ng, "Digital light field photography," Ph.D. dissertation (Stanford University, 2006).
7. G. Hauesler, "A method to increase the depth of focus by two step image processing," *Opt. Commun.* **6**, 38–42 (1972).
8. R. Raskar, A. Agrawal, and J. Tumblin, "Coded exposure photography: motion deblurring via fluttered shutter," in *Proceedings SIGGRAPH '06* (ACM, 2006), pp. 795–804.
9. J. Ojeda-Castañeda, E. Yezpez-Vidal, and C. M. Gómez-Sarabia, "Multiple-frame photography for extended depth of field," *Appl. Opt.* **52**, D84–D91 (2013).
10. H. H. Hopkins, "The aberration permissible in optical systems," *Proc. Phys. Soc. B* **70**, 449–470 (1957).
11. H. H. Hopkins, "Wave and ray aberrations," in *Wave Theory of Aberrations* (Oxford, 1950), pp. 12–16.
12. P. Mouroulis and J. Macdonald, *Geometrical Optics and Optical Design* (Oxford, 1997), pp. 206–208.
13. J. Ojeda-Castaneda and C. M. Gómez-Sarabia, "Key concepts for extending the depth of field with high resolution," *Opt. Pura Apl.* **45**, 449–459 (2012).
14. J. Ojeda-Castaneda and C. M. Gomez-Sarabia, "Tuning field depth at high resolution by pupil engineering," *Adv. Opt. Photon.* **7**, 814–880 (2015).
15. K. H. Brenner, A. W. Lohmann, and J. Ojeda-Castaneda, "The ambiguity function as a polar display of the OTF," *Opt. Commun.* **44**, 323–326 (1983).
16. A. Castro, J. Ojeda-Castaneda, and A. W. Lohmann, "Bow-tie effect: differential operator," *Appl. Opt.* **45**, 7878–7884 (2006).
17. J. Ojeda-Castaneda, L. R. Berriel-Valdos, and E. Montes, "Ambiguity function as a design tool for high focal depth," *Appl. Opt.* **27**, 790–795 (1988).
18. D. S. Barwick, "Efficient metric for pupil-phase engineering," *Appl. Opt.* **46**, 7258–7261 (2007).
19. E. R. Dowski, Jr. and W. T. Cathey, "Extended depth of field through wave-front coding," *Appl. Opt.* **34**, 1859–1866 (1995).
20. C. E. Cook and M. Bernfeld, *Radar Signals: An Introduction to Theory and Applications* (Artech House, 1993), pp. 59–108.
21. A. Castro and J. Ojeda-Castaneda, "Asymmetric phase masks for extended depth of field," *Appl. Opt.* **43**, 3474–3479 (2004).
22. A. Saucedo and J. Ojeda-Castaneda, "High focal depth with fractional power wavefronts," *Opt. Lett.* **29**, 560–562 (2004).
23. J. Ojeda-Castañeda, S. Ledesma, and C. M. Gómez-Sarabia, "Hyper Gaussian windows with fractional wavefronts," *Photon. Lett. Pol.* **5**, 23–25 (2013).

24. J. Liu, E. Miao, Y. Sui, and H. Yang, "Optimized non-integer order phase mask to extend the depth of field of an imaging system," *Opt. Commun.* **374**, 92–96 (2016).
25. J. Ojeda-Castaneda, "Comments on: "Optimized non-integer order phase mask to extend the depth of field of an imaging system" by Jiang Liu, Erlong Miao, Yongxin Sui, Huaijiang Yang," *Opt. Commun.* **381**, 443 (2016).
26. C. Varamit and G. Indebetouw, "Imaging properties of defocused partitioned pupils," *J. Opt. Soc. Am. A* **2**, 799–802 (1985).
27. T. C. Poon and M. Motamedi, "Optical-digital incoherent image processing for extended depth of field," *Appl. Opt.* **26**, 4612–4615 (1987).
28. A. Kolodziejczyk, S. Bara, Z. Jaroszewicz, and M. Sypek, "The light sword optical element—a new diffractive structure with extended depth of focus," *J. Mod. Opt.* **37**, 1283–1286 (1990).
29. N. Davidson, A. A. Friesem, and E. Hasman, "Holographic axilens: high resolution and long focal depth," *Opt. Lett.* **16**, 523–525 (1991).
30. J. van der Gracht, E. W. Dowski, M. G. Taylor, and D. M. Deaver, "Broadband behavior of an optical-digital focus-invariant system," *Opt. Lett.* **21**, 919–921 (1996).
31. S. Bradburn, W. T. Cathey, and E. R. Dowski, "Realizations of focus invariance in optical-digital systems with wave-front coding," *Appl. Opt.* **36**, 9157–9166 (1997).
32. R. Piestun, B. Spector, and J. Shamir, "Pattern generation with extended focal depth," *Appl. Opt.* **37**, 5394–5398 (1998).
33. H. B. Wach, E. R. Dowski, Jr., and W. T. Cathey, "Control of chromatic focal shift through wavefront coding," *Appl. Opt.* **37**, 5359–5367 (1998).
34. J. Ojeda-Castañeda and A. Saucedo, "Tunable focal depth by random superposition," *Opt. Mem. Neural Networks* **8**, 81–86 (1999).
35. W. Chi and N. George, "Electronic imaging using a logarithmic asphere," *Opt. Lett.* **26**, 875–877 (2001).
36. H. Wang and F. Gan, "High focal depth with a pure-phase apodizers," *Appl. Opt.* **40**, 5658–5662 (2001).
37. N. George and W. Chi, "Extended depth of field using a logarithmic asphere," *J. Opt. A* **5**, S157–S163 (2003).
38. W. Chi and N. George, "Computational imaging with the logarithmic asphere: theory," *J. Opt. Soc. Am. A* **20**, 2260–2273 (2003).
39. S. S. Sherif, W. T. Cathey, and E. R. Dowski, "Phase plate to extend the depth of field of incoherent hybrid imaging systems," *Appl. Opt.* **43**, 2709–2721 (2004).
40. X. Liu, X. Cai, S. Chang, and C. P. Grover, "Cemented doublet lens with an extended focal depth," *Opt. Express* **13**, 552–557 (2005).
41. G. Muyo and A. R. Harvey, "Decomposition of the optical transfer function: wavefront coding imaging systems," *Opt. Lett.* **30**, 2715–2717 (2005).
42. W. Chi and N. George, "Integrated imaging with a centrally obscured logarithmic asphere," *Opt. Commun.* **245**, 85–92 (2005).
43. S. Abrahamsson, S. Usawa, and M. Gustafsson, "A new approach to extended focus for high-speed, high-resolution biological microscopy," *Proc. SPIE* **6090**, 60900N (2006).
44. A. Greengard, Y. Y. Schechner, and R. Piestun, "Depth from diffracted rotation," *Opt. Lett.* **31**, 181–183 (2006).
45. E. Ben-Eliezer, E. Marom, N. Konforti, and Z. Zalevsky, "Radial mask for imaging systems that exhibit high resolution and extended depths of field," *Appl. Opt.* **45**, 2001–2013 (2006).
46. M. Somayaji and M. P. Christensen, "Enhancing form factor and light collection of multiplex imaging systems by using a cubic phase mask," *Appl. Opt.* **45**, 2911–2923 (2006).
47. A. Levin, R. Fergus, F. Durand, and W. T. Freeman, "Image and depth from a conventional camera with a coded aperture," *ACM Trans. Graph.* **26**, 70 (2007).
48. Q. Yang, L. Liu, and J. Sun, "Optimized phase pupil masks for extended depth of field," *Opt. Commun.* **272**, 56–66 (2007).
49. M. Somayaji and M. P. Christensen, "Frequency analysis of the wavefront coding odd-symmetric quadratic phase mask," *Appl. Opt.* **46**, 216–226 (2007).
50. G. Mikula, Z. Jaroszewicz, A. Kolodziejczyk, K. Petelczyc, and M. Sypek, "Imaging with extended focal depth by means of lenses with radial and angular modulation," *Opt. Express* **15**, 9184–9193 (2007).
51. A. Castro, Y. Frauel, and B. Javidi, "Integral imaging with large depth of field using an asymmetric phase mask," *Opt. Express* **15**, 10266–10273 (2007).
52. E. Garcia-Guerrero, E. R. Mendez, H. M. Escamilla, T. A. Leskova, and A. A. Maradudin, "Design and fabrication of random phase diffusers for extending the depth of focus," *Opt. Express* **15**, 910–923 (2007).
53. N. Caron and Y. Sheng, "Polynomial phase masks for extending the depth of field of a microscope," *Appl. Opt.* **47**, E39–E41 (2008).
54. P. Mouroulis, "Depth of field extension with spherical optics," *Opt. Express* **16**, 12995–13004 (2008).
55. H. Zhao, Q. Li, and H. Feng, "Improved logarithmic phase mask to extend the depth of field of an incoherent imaging system," *Opt. Lett.* **33**, 1171–1173 (2008).
56. J. Ojeda-Castaneda, E. Yépez-Vidal, and E. García-Almanza, "Complex amplitude filters for extended depth of field," *Photon. Lett. Pol.* **2**, 162–164 (2010).
57. K. Mitra, O. S. Cossairt, and A. Veeraraghavan, "A framework for analysis of computational imaging systems: role of signal prior, sensor noise and multiplexing," *IEEE Trans. Pattern Anal. Mach. Intell.* **36**, 1909–1921 (2014).
58. S. Pertuz, D. Puig, M. A. Garcia, and A. Fusiello, "Generation of all-focus images by noise-robust selective fusion of limited depth-of-field images," *IEEE Trans. Image Process.* **22**, 1242–1251 (2013).
59. J. R. Alonso, A. Fernandez, G. A. Ayubi, and J. A. Ferrari, "All-in-focus image reconstruction under severe defocus," *Opt. Lett.* **40**, 1671–1674 (2015).
60. J. Ojeda-Castañeda, J. E. A. Landgrave, and C. M. Gómez-Sarabia, "Conjugate phase plate use in analysis of the frequency response of imaging systems designed for extended depth of field," *Appl. Opt.* **47**, E99–E105 (2008).
61. M. Demenikov, G. Muyo, and A. R. Harvey, "Experimental demonstration of continuously variable optical encoding in a hybrid imaging system," *Opt. Lett.* **35**, 2100–2102 (2010).
62. J. Ojeda-Castaneda, E. Aguilera Gómez, H. P. Mora, M. T. Cisneros, E. R. L. Orozco, A. L. Martínez, J. S. P. Santamaría, J. G. M. Castro, and R. C. S. Segoviano, "Optical system with variable field depth," U.S. patent 8,159,753 (17 April 2012).
63. J. Ojeda-Castaneda, E. Yépez-Vidal, E. García-Almanza, and C. M. Gómez-Sarabia, "Tunable Gaussian mask for extending the depth of field," *Photon. Lett. Pol.* **4**, 115–117 (2012).
64. J. Ojeda-Castaneda, S. Ledesma, and C. M. Gómez-Sarabia, "Tunable apodizers and tunable focalizers using helical pairs," *Photon. Lett. Pol.* **5**, 20–22 (2013).
65. H. Zhao and J. Wei, "Tunable wavefront coded imaging system based on detachable phase mask: mathematical analysis, optimization and underlying applications," *Opt. Commun.* **326**, 35–42 (2014).
66. A. W. Lohmann, "Improvements relating to lenses and to variable optical lens systems formed by such lenses," British patent 998,191 (29 May 1964).
67. L. W. Alvarez, "Two-element variable-power spherical lens," U.S. patent 3,305,294 (3 December 1964).
68. M. L. Milne Thomson, *The Calculus of Finite Differences* (Macmillan, 1951).
69. S. Goldberg, *Introduction to Difference Equations* (Dover, 1986).
70. Taylor & Francis, <http://www.tandfonline.com/action/journalInformation?show=aimsScope&journalCode=gdea20>.
71. J. Ojeda-Castaneda, L. Ledesma, and R. Valencia, "Tunable hyperbolic apodizer," *Photon. Lett. Pol.* **7**, 11–13 (2015).
72. D. Compertore, A. Kingston, and I. Cox, "The area under the modular transfer function curve does not predict convolved E image quality," *Invest. Ophthalmol. Visual Sci.* **50**, 1554 (2009).
73. A. W. Lohmann, "Lentille de distance focale variable," French patent 1,398,351 (10 June 1964).
74. A. W. Lohmann, "Lente focale variable," Italian patent 727,848 (19 June 1964).